From a long-lived upper-crustal magma chamber to rapid porphyry copper emplacement: Reading the geochemistry of zircon crystals at Bajo de la Alumbrera (NW Argentina)

Yannick Buret[1]*, Albrecht von Quadt[1], Christoph Heinrich[1], David Selby[2], Markus Wälle[1], Irena Peytcheva[1,3]

[1]*Institute of Geochemistry and Petrology, Department of Earth Sciences, ETH Zürich, Clausiusstrasse 25, 8092 Zürich, Switzerland (*corresponding email: yannick.buret@erdw.ethz.ch)*
[2]*Department of Earth Sciences, Durham University, Durham DH1 3LE, United Kingdom*
[3]*Geological Instutute, Bulgarian Academy of Sciences, 1113 Sofia, Bulgaria*

Abstract

The formation of world class porphyry copper deposits reflect magmatic processes which take place in a deeper and much larger underlying magmatic system, which provides the source of porphyry magmas, as well as metal and sulphur-charged mineralising fluids. Reading the geochemical record of this large magmatic source region, as well as constraining the time-scales for creating a much smaller porphyry copper deposit, are critical in order to fully understand and quantify the processes which lead to metal concentration within these valuable mineral deposits. This study focuses on the Bajo de la Alumbrera porphyry copper deposit in Northwest Argentina. The deposit is centred on a dacitic porphyry intrusive stock that was mineralised by several pulses of porphyry magma emplacement and hydrothermal fluid injections. To constrain the duration of ore formation, we dated zircons from four porphyry intrusions, including pre-, syn- and post-mineralisation porphyries based on intersection relations between successive intrusion and vein generations, using high precision CA-ID-TIMS. Based on the youngest assemblages of zircon grains, which overlap within analytical error, all four intrusions were emplaced within 29 ka, which places an upper limit on the total duration of hydrothermal mineralisation. Re/Os dating of hydrothermal molybdenite fully overlaps with this high-precision age bracket. However, all four porphyries contain zircon antecrysts which record protracted zircon crystallisation during the ~ 200 ka preceding the emplacement of the porphyries. Zircon trace element variations, Ti-in-zircon temperatures, and Hf isotopic compositions indicate that the

four porphyry magmas record a common geochemical and thermal history, and that the four intrusions were derived from the same upper-crustal magma chamber. Trace element zoning within single zircon crystals confirms a fractional crystallisation trend dominated by titanite and apatite crystallisation. However zircon cathodoluminescence imaging reveals the presence of intermediate low luminescent (dark) growth zones in many crystals from all intrusions, characterised by anomalously high Th, U and REE concentrations and transient excursions in trace element ratios. A return to the same fractionation trend after this excursion excludes external compositional forcing such as magma mixing. Instead we interpret the "dark-zones" to record zircon crystallisation during a transient event of rapid growth that resulted from mafic magma injection into the base of the magma chamber, releasing a CO_2-rich vapour phase into the dacitic crystal mush. We propose that this vapour phase then migrated upwards to the apical part of the magma chamber from where it was expelled, together with successive batches of magma, to form the porphyry copper deposit within a short time-span of less than a few 10,000 years. The short duration of host rock emplacement, hydrothermal alteration and mineralisation presented in this study provides critical constraints on fluid storage in magma chambers and the genesis of large porphyry copper deposits.

1. Introduction

Porphyry Cu ± Mo ± Au systems represent focussed zones of intrusive activity, heat transfer, fluid-flow, mineral precipitation, and rock alteration of great economic significance, as well as of broader geological interest regarding the interface between the plutonic and volcanic domains of upper crustal hydrous magma systems. Porphyry copper deposits are composed of relatively small porphyritic stocks, commonly intruding the base of volcanoes, and located above larger magma chambers (Burnham and Ohmoto, 1980; Sillitoe, 2010). These are rarely exposed except by later dissection and tilting (Dilles, 1987), but more commonly documented by clear geophysical evidence (e.g. Steinberger et al., 2013). These large magma reservoirs are believed to be the main source of fluids, sulphur, and metals concentrated in porphyry Cu deposits (Candela, 1989), and it is therefore critical to understand the local and regional magmatic processes which underlie the deposits. When an underlying magma reaches fluid saturation, the fluids are thought to migrate upwards and concentrate in a cupola of the magma chamber. The accumulation of low-density magmatic fluids can lead to pressure build-up at the top of the magma body, triggering the sudden release of magma and fluids (Huber et al., 2012). These events are commonly repeated a number of times

within a single porphyry stock, resulting in several hydrothermal and magmatic pulses overprinting one another. Field relations of intersecting intrusion contacts and veins can therefore be used to bracket the timing of ore formation (von Quadt et al., 2011).

The timescales of the processes governing porphyry Cu formation have been widely studied but remain ambiguous, ranging from a few years based on modelling diffusive equilibration between fluids and rocks during alteration and vein mineral precipitation (e.g. Cathles and Shannon, 2007; Mercer et al., 2015), to tens of ka based on thermal modelling of the lifetime of upper-crustal magma chambers (Cathles, 1977; Weis et al., 2012) to the multi-million year life-time of magmatic complexes based on zircon U-Pb geochronology (e.g. Harris et al., 2004a). Recent high precision U-Pb zircon studies have used chemical abrasion – isotope dilution – thermal ionisation mass spectrometry (CA-ID-TIMS) analyses to suggest timescales of less than 100 ka of porphyry Cu formation (e.g. von Quadt et al., 2011; Chelle-Michou et al., 2014; Tapster et al., 2016). The common occurrence of accessory zircon in magmatic rocks, together with its refractory nature and low elemental volume diffusivities (Cherniak et al., 1997a; 1997b) make zircon invaluable to our understanding of upper crustal magmatic processes governing the generation of porphyry Cu deposits. *In-situ* zircon dating techniques provides high spatial resolution to target specific zones of individual zircons (e.g. cores and rims), but such techniques do not provide the necessary precision to resolve the timescales of Cu precipitation (Chiaradia et al., 2013).

CA-ID-TIMS U-Pb zircon geochronology has long been used to determine durations of magmatic processes (Schmitz and Bowring, 2001; Coleman et al., 2004; Glazner et al., 2004; Matzel et al., 2006; Miller et al., 2007; Schaltegger et al., 2009; Schoene et al., 2012; Wotzlaw et al., 2013; Rivera et al., 2014; Broderick et al., 2015). Improvements in zircon ID-TIMS geochronology by chemical abrasion (CA) to remove domains that suffer post-crystallisation Pb loss (Mattinson, 2005), the introduction of the well-calibrated EARTHTIME 2535 tracer solution (Condon et al., 2015; McLean et al., 2015), and a reduction of laboratory analytical blanks have improved the precision to the permil level on single $^{206}Pb/^{238}U$ zircon measurements (Schmitz and Schoene, 2007; von Quadt et al., 2016). Increased precision of individual $^{206}Pb/^{238}U$ measurements now resolves distinct zircon ages that span over 100 ka timescales within single rock samples in young magmatic systems (e.g. Bachmann et al., 2007; Miller et al., 2007). As a result of these observed clearly resolved temporal complexities, it is no longer valid to calculate weighted mean crystallisation ages of the entire zircon populations; instead, the youngest zircon(s) from a zircon population

within a single sample may be a better estimate of the eruption or emplacement age (Bachmann et al., 2007; Miller et al., 2007; Schoene et al., 2010a). Combining this variation in $^{206}Pb/^{238}U$ zircon dates with trace element and Hf isotopic compositions from the same volume of dated zircon can reveal important upper- or lower-crustal processes, including fractional crystallisation, magma mixing, mush rejuvenation and crustal assimilation on several hundred ka timescales (Wotzlaw et al., 2013; Broderick et al., 2015; Samperton et al., 2015).

In this study we obtain CA-ID-TIMS U-Pb zircon dates from pre-, syn- and post-ore porphyries which make up a geologically young porphyry copper deposit, with the aim of resolving durations of magmatic-hydrothermal ore formation. Our U-Pb zircon dates are supplemented by directly dating molybdenite from hydrothermal ore veins using the Re-Os chronometer. High-precision U-Pb zircon dates along with trace element and Hf isotope analyses, by solution inductively-coupled plasma mass spectrometry (ICP-MS), all from the same dated zircons are then combined with *in-situ* zircon geochemistry in order to track the magmatic processes which lead to large scale fluid exsolution, with the aim of understanding more quantitatively the processes of magma-chamber evolution, fluid exsolution and storage, and magmatic-hydothermal ore formation at the transition between the plutonic and volcanic environment.

2. Geological Setting

The Bajo de la Alumbrera deposit is part of the Farallón Negro volcanic complex (FNVC) in northwestern Argentina (Fig. 1). Magmatism in the FNVC is the easternmost manifestation of Neogene volcanism, occurring ~200 km inboard of the main magmatic arc as a result of the shallowing of the subducting slab (Allmendinger, 1986; Sasso and Clark, 1998).

The FNVC is considered to represent the remnants of a large stratocone volcanic complex, hosting numerous sub-volcanic intrusions and barren or mineralised porphyries (Llambías, 1972; Halter et al., 2004a). Whole rock and melt inclusion compositions from extrusive and intrusive samples from the FNVC range broadly in SiO_2 contents from basalt to rhyodacite (45 wt. % – <70 wt. %); between which almost all major and trace elements form linear arrays interpreted to represent binary mixing between mafic and felsic magmas, as supported by mixing and mingling textures between mafic and felsic magmas (Halter et al., 2004a, b). Magma mixing is further demonstrated by intra-sample compositional variations in melt inclusions from individual phenocryst phases, where more silicic compositions are recorded in plagioclase

and quartz, in contrast to the mafic melt inclusions which are restricted to amphibole and pyroxene (Halter et al., 2004b).

Based on Ar-Ar and U-Pb dating, magmatism occurred in the FNVC from ~9.7 Ma to ~6 Ma (Sasso and Clark, 1998; Halter et al., 2004a; Harris et al., 2004a). The early stage of magmatism (9.7 – 7.3 Ma) was dominated by extrusive volcanic activity composed of lava flows, flow breccias, with basaltic andesite to andesitic composition. Early intrusive units are also dominated by basaltic-andesite and andesitic rocks which have similar mineralogy to the volcanic units. Although intrusive magmatism occurs throughout the formation of the FNVC, it became the dominant type of magmatism during the later stages of the complex (7.3 – 6.0 Ma), when numerous stocks and dikes, ranging from several meters to 5 km in size intrude the overlying volcanic units (Llambías, 1972; Sasso and Clark, 1998; Halter et al., 2004a).

The ~7 Ma Bajo de la Alumbrera porphyry Cu deposit (Sasso and Clark, 1998; Harris et al., 2004a; von Quadt et al., 2011) comprises a composite stock of dacitic porphyries, with peripheral mineralisation extending into the surrounding volcanic rocks. Eight mappable intrusions form this stock (Proffett, 2003), including the pre-mineralisation P2 porphyry, the pre- to syn-mineralisation early P3 (EP3) porphyry, and the post-mineralisation late P3 (LP3) and P4 porphyries (Fig. 1). The P4 porphyry corresponds to the postmineral dikes in the terminology of Proffett (2003). The relative timing of each porphyry can be distinguished using cross-cutting field relationships which are observed as sharp contacts between the porphyry intrusives, with later magmas truncating veins in the earlier magmatic rock (Fig. 2). All intrusions are strongly porphyritic with the matrix forming 40 to 70 vol% of the rocks. There is a general temporal evolution from early silica-rich dacites containing phenocrysts of plagioclase (10-40%), quartz (1-6%), biotite (1-6%) and hornblende (1-5%) to later intermediate andesitic intrusions containing phenocrysts of plagioclase (10-15%), quartz (1-2%), biotite (2-5%) and hornblende (10%), during the construction of the stock (Ulrich and Heinrich, 2002; Proffett, 2003). All porphyry intrusions contain accessory phases of magnetite, zircon, apatite and titanite. The evolution from early silicic dacite intrusions to more intermediate andesitic intrusions has been interpreted as evidence for a chemically structured upper crustal magma chamber, with the extraction of silica-rich melts from the upper portions followed by the extraction of the deeper, more mafic units from the hybrid magma chamber (Halter et al., 2004b; 2005).

The two earliest intrusions (P2 and EP3) host all the economic Cu ore grade, containing an average grade of 0.54 % Cu and 0.64 g/t Au (Fig. 1) and are also the most altered porphyries in the stock. The LP3

and P4 porphyries are considered post-mineralisation since they do not host economic Cu ore grades and they cross-cut all hydrothermal quartz veins in the mineralised P2 and EP3 porphyries (Fig. 2). Molybdenite is subordinate in the Bajo de la Alumbrera and its distribution is restricted to a ring in the outermost part of the deposit, commonly in the surrounding volcanics. Some molybdenite is observed in quartz – anhydrite veins which cross-cut the EP3 porphyry (Proffett et al., 2003). The P2 porphyry intrusion is the most densely veined intrusion (20-50%), and displays pervasive quartz-magnetite and intense potassic alteration. Subsequent intrusions become progressively less altered from pervasive potassic alteration in the EP3 porphyry to weak feldspar-destructive alteration in the post mineralisation P4 porphyries, which correlates with a significant decrease in the vein density of the post-mineralisation porphyries (Ulrich and Heinrich, 2002; Proffett, 2003). The decrease in alteration and veining intensity for the later intrusions is consistent with the waning of the magmatic hydrothermal system (Ulrich and Heinrich, 2002). The deeper, more central parts of these porphyries are extensively veined and altered, however these regions of the deposit do not host economic ore grades (Fig. 1; Ulrich and Heinrich, 2002; Proffett, 2003). Ore-metal enrichment is concentrated in an annular zone closing near the top of the deposit and diminishing in metal grade with depth (Fig. 1). This ore-shell surrounds a barren core that is highly veined and altered but metal-poor, a typical geometry considered to form as a result of steep temperature and fluid pressure gradients between an overpressured magmatic fluid plume and the hydrostatic pressure domain of the volcano (Weis et al., 2012).

3. Samples and Methods

Representative samples of the P2, EP3, LP3 and P4 porphyries for this study were collected based on mine maps and clear cross-cutting relationships from various locations within the Bajo de la Alumbrera mine (See Supplementary Materials for sample locations). Two EP3-hosted molybdenite samples were collected from the 52-51.1 drill-core, from the outer-part of the deposit. The molybdenite occurs in quartz-anhydrite-gypsum veins (as described in Proffett, 2003) also containing minor chalcopyrite. We saw no evidence of molybdenite hosted in the post-mineralisation porphyries (LP3 and P4). Zircons were separated from all porphyry samples and molybdenite was separated from the quartz-anhydrite-molybdenite vein using conventional techniques. One aliquot of zircons from each sample was selected for CA-ID-TIMS and analysed using the Thermo TritonPlus at ETH Zurich. Data reduction and error propagation of high precision

U-Pb CA-ID-TIMS zircon dates was carried out using Tripoli and U-Pb Redux software (Bowring et al., 2011) applying the algorithms of McLean et al. (2011).

To observe the geochemical evolution of the zircons through time, the "wash" from the dated zircon grains were analysed for trace elements (modified after Schoene et al., 2010b) and Hf isotopes at ETH Zurich, using the Element Sector Field (SF)-ICP-MS and Nu Instruments Multi Collector (MC)-ICP-MS, respectively. In order to obtain spatially resolved geochemical information a second zircon aliquot was mounted in epoxy and polished to obtain cathodoluminescence (CL) images using a Tescan EOscan VEGA XLSeries 4 Secondary electron microscope (SEM) at the Department of Material Science, ETH Zurich, prior to *in-situ* trace element analysis using a 193 nm Resonetics ArF excimer laser coupled to an Element SF-ICP-MS and Hf isotope analysis using a 193 nm GeoLas laser coupled to a Nu Instruments MC-IC-ICP-MS at ETH Zurich. The Re and Os abundance and isotopic compositions of two molybdenite concentrates were determined at the University of Durham using a Thermo Triton mass spectrometer and the mineralisation age of the molybdenite was calculated using the decay constant of Smoliar et al. (1996). Detailed analytical procedures are described in the Supplementary Materials.

4. Results

4.1. ID-TIMS U-Pb zircon and Re-Os molybdenite geochronology

A total of 70 single zircon crystals from the four porphyry intrusions (P2, EP3, LP3, P4) in the Bajo de la Alumbrera deposit have been dated using CA-ID-TIMS (Fig. 3; Supplementary Materials Table 1).

All four of the Bajo de la Alumbrera porphyries analysed contain zircon dates spanning a clearly resolved variation of ~200 ka, which precludes the calculation of a geologically meaningful or statistically significant weighted mean age from the entire zircon population of any one porphyry intrusion. The youngest zircons from each sample which correspond to a single population, within a 95% confidence interval (Wendt and Carl, 1991), were use to calculate the interpreted age of emplacement of each porphyry. Thirty-six zircons were analysed from the pre- (syn-) mineralisation P2 (n=19) and EP3 (n=16) porphyries. The youngest zircon from the P2 (7.097 ± 0.013 Ma) and EP3 (7.073 ± 0.048 Ma) porphyries yield dates that overlap within analytical uncertainties. The five youngest $^{206}Pb/^{238}U$ zircon dates from the P2 porphyry are statistically equivalent with a weighted mean date of 7.1102 ± 0.0093 Ma (MSWD = 2.1; 2 sigma), with the

eight youngest statistically equivalent $^{206}Pb/^{238}U$ zircon dates from the EP3 porphyry yielding a slightly younger, but overlapping weighted mean date of 7.1022 ± 0.0075 Ma (MSWD = 1.7; 2 sigma). The slight difference in the overlapping emplacement ages are in agreement with the cross-cutting relationships between both mineralised porphyries and constrain the upper limit of the age of mineralisation. Similarly, thirty-six zircons were analysed from the post-mineralisation LP3 (n=16) and P4 (n=19) porphyries and also record a period ~200 ka of zircon crystallisation, that broadly overlaps with the pre- (syn-) mineralisation porphyries (P2 and EP3). The youngest single zircon crystal from the post-mineralisation porphyries yields overlapping emplacement ages of 7.067 ± 0.021 Ma and 7.087 ± 0.012 Ma for the LP3 and P4 porphyry intrusions, respectively. The eight youngest $^{206}Pb/^{238}U$ zircon dates from the LP3 porphyry can be interpreted as a single zircon population yielding a weighted mean age of 7.0963 ± 0.0085 Ma (MSWD = 1.7; 2 sigma), which is indistinguishable from the seven youngest P4 zircons with a weighted mean date of 7.0994 ± 0.0063 Ma (MSWD = 1.6; 2 sigma). The geochronology results of this study in comparison with previous work on the Bajo de la Alumbrera porphyry Cu deposit are discussed in the Supplementary Materials.

Two molybdenite veins from the EP3 porphyry yield almost identical Re-Os dates of 7.093 ± 0.036 Ma and 7.084 ± 0.036 Ma (uncertainty includes the decay constant uncertainty; Supplementary Materials Table 2). Both samples have Re concentrations of 1133 and 1116 ppm respectively, thus minimising any potential effect of any common Os on the obtained dates. The averaged Re-Os mineralisation age of 7.089 ± 0.025 (n = 2) is in excellent agreement with the porphyry emplacement ages calculated from the high-precision zircon U-Pb dates (Fig. 3).

4.2. Bulk grain solution trace element and Hf-isotopic compositions of zircons

Zircon trace element and Hf-isotopic compositions were obtained from the same zircon volume dated by CA-ID-TIMS, using the TIMS-TEA technique (Fig. 4; modified after Schoene et al., 2010b) and by *in-situ* LA-ICP-MS after careful textural characterisation other zircons from the same sample (Figs. 5, 6). Together, both methods permit comparison of the geochemical signatures to the high-precision U-Pb zircon dates (TIMS-TEA), as well as textural information obtained from zircon CL images of the zircons (Fig 5; *in-situ* LA-ICP-MS). The TIMS-TEA and *in-situ* results are summarised in Figures 4, 6 and in Supplementary Material Tables 3 - 6.

Zircons from all four porphyry intrusions are indistinguishable in terms of geochemistry and compositionally overlap throughout the full range of trace elements and isotopic compositions. Two grains from the P2 porphyry were omitted from the plots due to elevated LREE concentrations, which we attribute to an accessory mineral inclusion in these grains. Whole grain trace element concentrations display non-systematic temporal variations (Fig. 4), which shows variable liquid compositions at the same time. Bulk zircon grain Hf isotopic compositions yield values ranging from εHf = -4.7 to +5.8, with the majority of the data ranging between -3 and 0 (Fig. 4d). Based on Hf isotopes in zircon no distinction can be made between the different porphyry units and there is no clear temporal trend.

4.3. Zircon textures

Based on the common occurrence of low luminescent growth zones ("dark-zones") observed in zircon CL images (Fig. 5) we subdivide zircons for geochemical analyses into two groups. Group 1 zircons, which are the most common, contains zircons that lack "dark-zones" and display continuous growth zoning (Fig. 5a, c, e, g). Group 2 zircons contain the "dark-zones" (Fig. 5 b, d, f, h) and are subsequently subdivided into three zones. The grain interiors (cores) are typically characterised by growth zoning and exhibit the least evolved geochemical signatures (e.g. low Yb/Gd and high Th/U ratios). The "dark-zones" in CL are commonly enriched in trace elements, containing up to several thousand ppm Th and U. These zones are also characterised by elevated Hf concentrations (up to 15,000 ppm) and often display more evolved $(Yb/Gd)_N$ and Th/U ratios (Fig 5). The "dark-zones" are also characterised by non-systematic trace element behaviour with regards to fractionation trends. The contacts at either side of the "dark-zones" are typically sharp and sometimes exhibit some resorption textures on the rim-ward side. The zircon rims which overgrow the "dark-zones" are characterised fine growth zoning. In contrast to the "dark-zones", their geochemical signatures more closely match that of the zircon cores, albeit more evolved (Fig. 6). The Group 1 zircons overlap in geochemical space with the cores and rims from Group 2 zircons.

4.4. In-situ trace element and Hf isotope analyses

Results of the *in-situ* analyses are presented in Figure 6 and in Supplementary Materials Figure 1. Despite the lack of trace element trends through time, covariation diagrams from both *in-situ* and TIMS-TEA analyses point to zircon crystallisation from a fractionating magma chamber, where titanite and apatite were

252 the dominant phases controlling the trace element budget of the magma (Fig. 6). The presence of co-
253 crystallising titanite and apatite results in REE depletions within a magma, showing an increase in $(Yb/Gd)_N$
254 and a decrease in Th/U ratios (Fig. 6a, b; Reid et al., 2011; Wotzlaw et al., 2013), and an increase in Ce/Sm
255 (Fig. 6c, d) and Eu/Eu* (Fig. 6e, f). This is in agreement with abundant accessory titanite and apatite found
256 in all porphyry intrusions and a decrease in the Ti concentration of bulk rock compositions towards more
257 evolved compositions (Halter et al., 2004a).

258 Bulk grain trace element ratios for the most part correlate with the rim ratios (Fig. 6), with the
259 exception of the LREEs, which tend to overlap with the cores rather than the rims (Fig. 6c, d). While higher
260 REE concentrations zircon cores compared to the volumetrically larger rim could explain the elevated LREE
261 concentrations in the bulk grains relative to the zircon rims, it does not explain why the bulk grain MREE
262 and HREE concentrations correspond more closely to the rims. We therefore propose that micro-melt, or
263 mineral (e.g. apatite, titanite) inclusions present in the dated zircon grains resulted in the elevated LREEs
264 (Reid et al., 2011). Mineral inclusions, especially apatite, and melt inclusions are common within zircons
265 from all of the analysed samples and while significant efforts were made to avoid dating zircons which
266 contained inclusions, it is likely that some micro-inclusions were present in some of the bulk zircon grains
267 analysed. This is supported by the ubiquitous presence of comparatively high La concentrations (1-5 ppm) in
268 the dated zircons relative to the zircons analysed by LA-ICP-MS and to standard zircons (Temora-2 and
269 91500), which yield La concentrations of below 0.1 ppm (See Supplementary Materials Tables 2, 3). We
270 also suggest that these inclusions have a minimal effect on the MREEs and HREEs due to the high
271 concentrations of these elements in zircons. Furthermore the effect of these inclusions on the obtained U-Pb
272 zircon dates should be minimal since there is no evidence that any of the analysed common Pb (e.g. elevated
273 ^{204}Pb) was derived from the zircons, based on routine total procedural blank measurements (Supplementary
274 Materials).

275 Titanium-in-zircon thermometry (Watson and Harrison, 2005; Watson et al., 2006; Ferry and
276 Watson, 2007) permits the determination of the temperatures at which zircons crystallise in evolving
277 magmas (Claibourne et al., 2010; Reid et al., 2011). The presence of magmatic quartz in the Bajo de la
278 Alumbrera porphyries suggests that the silica activity (a_{SiO2}) was ~1. Based on the presence of magmatic
279 titanite we apply an a_{TiO2} of 0.7 (Chelle-Michou, 2014). A high Ti background (~4 ppm) in one analytical
280 session resulted in some Ti values falling below the detection limit. Temperatures calculated for all

porphyries yield comparable values, ranging from 750 °C to 650 °C and show overall core-rim cooling trends (Fig. 6g, h). This temperature range is similar to other Ti-in-zircon thermometry obtained from other porphyry systems (Chelle-Michou, 2014).

In order to relate Hf isotopic composition in zircon to textural information, cores and rims were analysed. Data from zircon cores from all porphyries range from εHf = -5.0 to 0 (average = -2.8; n = 49). Zircon rims show εHf values ranging from -4.2 to 0.4 (average = -2.1 n = 49). Despite the minor differences between the cores and rims, they cannot be distinguished based on the uncertainty of the measurements (± 1 εHf unit; Supplementary Materials Table 6).

5. Discussion

5.1. Effect of mixing various age domains on obtained CA-ID-TIMS dates

A large spread of zircon dates that cannot be explained by analytical uncertainty is common in many igneous systems (e.g. Miller et al., 2007; Schoene et al., 2010a; Wotzlaw et al., 2013). This dispersion can be interpreted to reflect one of the following processes: 1) Post-crystallisation Pb-loss; 2) A variable mixture of two age domains (e.g. an older core overgrown by a younger rim) within individual zircon grains; or 3) Protracted but individually rapid crystallisation of zircon crystals in a long-lived magmatic reservoir.

The removal of Pb-loss domains by chemical abrasion is assumed to be highly effective in young samples and therefore any residual Pb-loss domains would have a negligible affect on the final zircon date. Furthermore the similar spread in zircon dates within all samples, and the fact that the cross-cutting sequence is supported by the crystallisation age of the youngest zircon from each porphyry intrusion, suggests that the dispersion of zircon dates is unlikely to be the result of later Pb-loss. Based on continuous intragrain geochemical trends, together with the intergrain overlap between cores and rims suggests that the spread in zircon dates is not the result of a variable mixing between two distinct age domains, where one would expect clear distinctions between cores and rims on an intergrain level, which would be resolvable even by LA-ICP-MS. It is therefore very likely that the ~200 ka spread in our geochronology dataset reflects continuous zircon growth in a magma body. Heat loss imposes that small porphyry intrusions crystallise within a few thousand years (e.g. Cathles, 1977). The ~200 ka spread of U-Pb zircon dates in the four porphyry units therefore cannot be the result of *in-situ* zircon growth after porphyry emplacement, but rather reflects

protracted zircon crystallisation in a larger upper crustal magma chamber located below the emplacement of the porphyry intrusions (Sillitoe, 2010). The youngest zircons are inferred to have formed in the magma chamber immediately prior to porphyry extraction, and therefore represent the most likely (although strictly speaking, the maximum) age of porphyry emplacement.

In addition we must consider how the "dark-zones", observed in CL images (Fig. 5), which contain up to 7,000 ppm U (Fig. 7) may effect our interpretations. The presence of the “dark-zones” in the Group 2 zircons is likely the result of elevated U^{4+} concentrations, which suppresses the CL emission caused by the HREEs in zircon (Ohnenstetter et al., 1991). These high U concentrations in these zones have the potential to bias the obtained CA-ID-TIMS U-Pb zircon date towards the "dark-zones" instead of being weighted towards the higher volume, younger rim, which would be true in the case of similar U concentrations throughout a single zircon crystal (Samperton et al., 2015). All zircon crystals selected for CA-ID-TIMS were dissolved as whole crystals and unfortunately we do not have CL information for the dated grains and cannot relate the differing textures seen in both zircon groups to the temporal variations in geochemistry (Fig. 4). However, Figure 7 demonstrates that the U concentration from the dated zircons (140 ppm - 710 ppm; average = 325 ppm; n = 72) more closely resemble the U concentrations from the *in-situ* analysed rims (zircon exteriors; 100 ppm - 900 ppm; average = 323 ppm; n = 203). We therefore conclude that the dated zircons either did not contain these high U "dark-zones", the "dark-zones" were effectively removed by chemical abrasion (Mattinson, 2011) or that the "dark-zones" did not have a significant impact on the acquired zircon U-Pb dates. Furthermore, the similar U concentrations of the zircon cores and rims would suggest that the CA-ID-TIMS U-Pb zircon dates are in fact weighted towards the volumetrically dominant outer zones (see discussion in Samperton et al., 2015), and there is only a small contribution from the volumetrically smaller core of the zircons.

5.2. Timescales of porphyry Cu formation

Given that the observed spread of U-Pb zircon dates represents protracted zircon crystallisation in an evolving magma chamber (see discussion above), the youngest zircon grain, or population of zircon grains from each porphyry should represent the closest approximation of the emplacement age of that porphyry. Previous studies have advocated the use of the youngest zircon grain to approximate the eruption / emplacement of magmas (e.g. Bachmann et al., 2007; Schoene et al., 2010a; von Quadt et al., 2011). This

approach is subject to the risk that a single youngest zircon measurement may be subject to an uncorrected error, e.g., due to incomplete removal of a crystal domain that experienced later Pb loss. On the other hand, a mean age of the youngest statistically equivalent population of zircon dates from a single porphyry intrusion will yield a more precise emplacement age, although the accuracy of this calculated age may be compromised by slightly older zircons that are included in the calculation. Regardless of which approach we use, both the youngest zircon and the youngest population of zircons from each porphyry intrusion yields almost identical timescales of porphyry copper formation in Bajo de la Alumbrera (Fig. 3).

Since all porphyry intrusions yield a population of several youngest, overlapping, statistically equivalent zircon dates (Fig. 3), we can precisely constrain the emplacement age of each porphyry. The strong variation in zircon geochemistry for the youngest zircon population (Fig. 4) from each porphyry suggests that the zircons grew from variable liquid compositions at the same time, a feature that has been previously shown through Sr isotope variations within a single thin-section (Charlier et al., 2007). Moreover, the calculated emplacement ages can be used to constrain the maximum time-span of the formation of the Bajo de la Alumbrera porphyry stock, thus bracketing the hydrothermal pulses which resulted in Cu precipitation. Using the maximum difference (including analytical uncertainties) between the emplacement age of the oldest, mineralised porphyry intrusion (P2) and the emplacement age from a latest post-mineralisation porphyry intrusion (P4) we conclude that the maximum time-span for the formation of the porphyry stock was 29 ka (Fig. 3), during which time all of the economic ore (including the molybdenite at 7.089 ± 0.025; Fig. 3) was precipitated. Using the more conservative approach of applying the youngest zircon from the earliest (P2) and latest (P4) porphyry intrusions yields a similar duration of 35 ka. These time-spans, however, incorporate the maximum uncertainties associated with each porphyry emplacement age, and since the emplacement of all porphyry intrusions temporally overlapped, the period of porphyry Cu formation in the Bajo de la Alumbrera deposit may have been significantly shorter than our U-Pb zircon estimations. Our timescale, based on high-precision CA-ID-TIMS zircon dates is also supported by recent numerical modelling approaches which suggest a timescale of porphyry Cu formation within a single porphyry stock of between 50 and 100 ka (Weis et al., 2012).

5.3. Evolution of the ore forming magma chamber

High-precision dating studies combined with detailed field mapping have demonstrated that many upper crustal plutons and batholiths are constructed by the incremental addition of small magma batches over several ka to Ma timescales (Coleman et al., 2004; Glazner et al., 2004; Memeti et al., 2010; Schoene et al., 2012; Wotzlaw et al., 2013; Broderick et al., 2015; Samperton et al., 2015). Protracted timescales of zircon growth, combined with zircon compositions, gives zircon the potential to record the evolution of an ore forming magma chamber from zircon saturation through to porphyry emplacement and solidification. While zircon/melt partition coefficients are to some extent temperature dependent (Rubatto and Hermann, 2007), the geochemical compositions of zircons also primarily reflect the melt composition at the time of zircon crystallisation (Claibourne et al., 2010; Miller et al., 2011; Reid et al., 2011; Wotzlaw et al., 2013; Rivera et al., 2014; Samperton et al., 2015), which is strongly influenced by co-crystallising phases and the oxidation state of the magma. During the 200 ka of zircon crystallisation, zircon geochemistry from the four porphyries varies measurably but shows no clear temporal trends (Fig. 4), suggesting that the magma chamber underlying the Bajo de la Alumbrera porphyries was not a well-mixed single melt reservoir that thermally contracted with time. During the evolution of the magma chamber, zircons record an overall increase in trace element variability, which could be related to different degrees of crystallinity throughout the magma chamber and zircons crystallising within increasingly isolated melt pockets in a larger magmatic body. Moreover, both the bulk grain analyses and *in-situ* LA-ICP-MS analyses show that zircons record inter- and intra-grain trends which can be explained by coeval crystallisation of zircon, titanite and apatite in a cooling and fractionating magma chamber (increasing Yb/Gd_N, decreasing Th/U and Ti; Fig. 6; Fig. 8b). The similarity of the geochemical trends, trace-element dispersions and $^{206}Pb/^{238}U$ age spectra of the zircons suggests a common derivation of all four porphyry intrusions from a single magma body.

Previous studies have suggested that zircon may record the oxidation state of the magma from which it has grown, on the basis of Ce and Eu anomalies (Ballard et al., 2002; Burnham and Berry, 2012; Trail et al., 2012; Chelle-Michou et al., 2014; Dilles et al., 2015). The presence of titanite and plagioclase in the Bajo de al Alumbrera porphyries makes the signal from these anomalies convoluted (Fig 5c-f), due to the preferential uptake of middle REEs in titanite compared to the heavy and light REEs and the preferential incorporation of Eu^{2+} by plagioclase. Titanite therefore has the effect of decreasing the magnitude of the Eu

anomaly (which is counter-balanced by extensive plagioclase crystallisation) recorded in the zircon, due to the lower distribution coefficients of Eu relative to Sm and Gd in titanite (Deering and Bachmann, 2010). The calculation of a Ce anomaly is challenging due to the low concentrations of La and Pr in zircon and has prompted the use of Ce/Nd or Ce/Sm ratios in zircon as potential recorders of the changing oxidation state of the magma (Chelle-Michou et al., 2014). However titanite crystallisation, which has higher distribution coefficients of MREEs compared to LREEs, may cause the residual melt to be enriched in Ce relative to Nd and Sm. Without the direct measurement of the true Ce^{4+}/Ce^{3+} ratio (Trail et al., 2015) estimations of the oxidation state of a magma from the Ce anomaly in zircons should be treated with caution as they can be strongly influenced by the crystallising assemblage. In the case of Bajo de la Alumbrera the coeval crystallisation of titanite, apatite and plagioclase, together with zircon, indicates that the Eu and Ce anomalies are unlikely to provide information about the oxidation state of the magma from which the zircon grew.

While the overall zircon geochemical evolution indicates a cooling fractionating magma chamber, the geochemical signatures from the low luminescent "dark-zones" do not correlate with the fractional crystallisation trends defined by the intragrain core-rim variations (Fig. 8c). We therefore propose that the observed "dark-zones" are the result of either: 1) Elemental diffusion within the zircon crystal; 2) Crystallisation in a cooling crystal-rich magma, followed by magma recharge (e.g. zircon rims); or 3) Kinetically controlled non equilibrium crystal-melt partitioning of trace elements into the crystallising zircons (e.g. Hoffmann et al., 2009).

Since elemental diffusivities in zircons is extremely slow, even at magmatic temperatures (Cherniak et al., 1997a, 1997b), it is unlikely that the geochemical anomolies observed in the "dark-zones" are the result of elemental diffusion. In the second case, we consider that if equilibrium mineral/melt partitioning increases corresponding to decreasing temperatures and with increasing silicic melt compositions (Rubatto and Hermann, 2007) an increase in zircon trace-element concentrations should be observed in a cooling magma, if co-crystallising phases are ignored. This is in agreement with our trace element fractional crystallisation trends at low temperatures (Ti-in-zircon <700 °C; Fig. 6g, h) and with the observed enrichment of Th, U, Hf and REEs within the "dark-zones" (Fig. 6; Fig 8). Previous studies have suggested that the Bajo de la Alumbrera deposit was formed as a result of magma mixing between two compositional end-members (<50 % SiO_2 and > 70 % SiO_2), but these are based on melt inclusions and refer to the longer-

term evolution of the entire FNVC (Halter et al., 2004a, b; 2005). In this study of a single porphyry stock, we show that zircon rims follow coherent core-rim trends when the "dark-zones" are excluded, i.e., these excursions are only transient (Fig. 8). Furthermore, the rims which overgrow the "dark-zones" do not record a significant geochemical modification to the magma reservoir (e.g. zircon rims show higher degrees of fractionation than the cores). These observations indicate that the anomalous geochemical signatures of the "dark-zones" do not occur due to temperature fluctuations or changes in bulk melt chemistry, as described in zircon studies from unmineralised plutons or volcanic eruptions (Claiborne et al., 2010; Wotzlaw et al., 2013; Broderick et al., 2015). We therefore propose that the geochemically anomalous "dark-zones" observed in the zircons are the result of kinetically controlled disequilibrium crystallisation related to rapid zircon growth.

To summarise, during 200 ka of zircon crystallisation at Bajo de la Alumbrera, zircons record cooling fractionation trends from compositionally distinct magma batches that existed over the evolution of the magma chamber. While zircons reflect cooling and fractionation trends, the "dark-zones" observed in zircon is unlikely to reflect processes such as changing oxidation state and/or mafic-felsic magma mixing events. We therefore propose that the observed "dark-zones" most likely grew as the result of kinetically controlled disequilibrium crystallisation due to rapid zircon growth.

5.4. Forming a world-class porphyry Cu deposit

Based on the data presented we propose the following model linking the formation of the Bajo de la Alumbrera porphyry Cu deposit to the evolution of zircon-crystallisation within an upper crustal magma chamber (Fig. 9).

(a) At ~7.35 Ma zircons in a hydrous, fluid-saturated upper crustal magma chamber began crystallising (Fig. 3; Fig. 9a). Zircons from this period record crystallisation in a cooling magma (Ti-in-zircon thermometry <750 °C; Fig. 6e, f), exhibit continuous growth zoning (Fig. 5), as well as fractional crystallisation trends controlled by co-crystallising titanite and apatite (Fig. 6).

(b) Injection of a hotter, more mafic magma (cf. Halter et al., 2004a) was quenched at the boundary with the cooler felsic mush (T = 650°-750 °C; Fig. 6g, h), resulting in the exsolution of volatiles from the mafic magma into the overlying felsic mush, due to decompression as well as crystallisation (‘first’ and ‘second’ boiling; Fig. 9b; Bachmann and Begantz, 2006; Huber et al., 2012). The fluid exsolved from the

underplated mafic melt would likely have higher CO_2/H_2O than the fluid exsolved from the overlying felsic mush (Botcharnikov et al., 2005) and would therefore decrease the H_2O solubility in the felsic mush from which the zircons are growing (Wark et al., 2007). This decrease in the H_2O solubility, which occurred in the parts of the magma chamber where the upwelling CO_2-rich vapour phase was most focussed, resulted in the rapid growth of zircon crystals recorded by the "dark-zones". As the mixed H_2O-CO_2-rich vapour reached equilibrium with the resident felsic magma, the geochemical effect of the CO_2-rich fluid would diminish and "normal" crystal growth would resume. This model is consistent with many recent studies which imply that the sulphur and metals required to form a world class porphyry Cu deposit must be sourced from a more mafic magma (Hattori, 1993; Hattori and Keith, 2001; Halter et al., 2005; Zajacz and Halter, 2009; Nadeau et al., 2013). High degrees of crystallinity could result in the formation of connected fluid pathways, which allowed the vapour phase to rapidly migrate towards the apical parts of the magma chamber (Fig. 9b; Huber et al., 2012). A lack of evidence for thermal rejuvenation of the crystallising felsic mush from the zircon geochemistry and consistently low Ti-in-zircon temperatures (Figs. 4, 5, 8) suggest that large scale magma remobilisation did not occur. Although dissolution features recorded in zircons are rare, the presence of embayed quartz crystals in Bajo de la Alumbrera, which contain abundant primary fluid inclusions (Harris et al., 2004b) may be evidence for remobilisation of the felsic mush immediately prior to porphyry copper formation (Tapster et al., 2016).

(c) At ~7.1 Ma fluid overpressure resulted in fluids and magma being released into the overlying hydrothermal system through pressure build-up at the apical parts of the magma chamber (Burnham and Ohmoto, 1980; Sillitoe, 2010). Zircons were "tapped" from different parts of the composite magma chamber in quick succession, forming multiple porphyries with an extended zircon age spectrum within a short period of less than 35 ka (Fig. 3). Magmatic fluids expelled within the same period formed the present day ore-shell (Figs. 1, 9c).

6. Summary and Conclusions

We have tracked the geochemical evolution of an ore forming magma chamber, from zircon saturation to the formation of an economic porphyry Cu deposit. By combining protracted U-Pb zircon growth histories with the *in-situ* zircon geochemistry we document the presence of a large-scale upper-crustal magma chamber which gradually cooled during 200 ka of zircon growth. Geochemical variability in

zircon, throughout the lifetime of the magmatic system, is consistent with zircon crystallisation in an upper crustal chamber which was in a highly crystalline, immobile state. An input of CO_2-rich fluid from a mafic recharge event, recorded by a period of rapid growth in the zircon crystals, triggered fluid saturation and may have provided additional metals and sulphur to the formation of the porphyry Cu deposit. We suggest that a high degree of crystallinity in the felsic crystal mush may have been critical in forming the Bajo de la Alumbrera ore deposit, as it would have allowed the formation of connected fluid pathways which could quickly drain the upper parts of magma chamber. Future work relating complex zircon textures with high precision CA-ID-TIMS geochronology could provide further insights into these complex magmatic systems. After the extended upper crustal magma residence time (200 ka), the four porphyry intrusions and two phases of hydrothermal mineralisation rapidly occurred within 29 ka, though these timescales may be significantly shorter. To our knowledge, these are the shortest timescales obtained using geochronology for the formation of any porphyry Cu deposit and provide critical constraints on the physical hydrology of magma – fluid – rock interactions during ore formation.

7. Acknowledgements

This work was supported through the SNF project 200021-146651. We are grateful for the extensive logistical support provided by Minera Alumbrera Ltd. and Glencore. We would particularly like to thank Ariana Carrazana Di Lucia for her help during the field season in 2013. We would like to thank André Röthlisberger for his technical help during the research. Helpful input at various stages of the project from Olivier Bachmann, Jörn Frederik Wotzlaw, Cindy Broderick and Ben Ellis is gratefully appreciated. Reviews of John M. Hanchar, Tom Sisson, an anonymous reviewer and the editorial comments by Tamsin Mather helped improving an earlier version of this manuscript.

8. References

Allmendinger, R.W., 1986. Tectonic development, southeastern border of the Puna Plateau, northwestern Argentine Andes. Geological Society of America Bulletin 97, 1070-1082.

Bachmann, O., Bergantz, G.W., 2006. Gas percolation in upper-crustal silicic crystal mushes as a mechanism for upward heat advection and rejuvenation of near-solidus magma bodies. Journal of Volcanology and Geothermal Research 149, 85-102.

Bachmann, O., Oberli, F., Dungan, M., Meier, M., Mundil, R., Fischer, H., 2007. $^{40}Ar/^{39}Ar$ and U-Pb dating of the Fish Canyon magmatic system, San Juan Volcanic field, Colorado: Evidence for an extended crystallization history. Chemical Geology 236, 134-166.

Ballard, J.R., Palin, M.J., Campbell, I.H., 2002. Relative oxidation states of magmas inferred from Ce (IV)/Ce (III) in zircon: application to porphyry copper deposits of northern Chile. Contributions to Mineralogy and Petrology 144, 347-364.

Botcharnikov, R., Freise, M., Holtz, F., Behrens, H., 2005. Solubility of C-O-H mixtures in natural melts: new experimental data and application range of recent models. Annals of Geophysics 48, 633-646.

Bowring, J., McLean, N.M., Bowring, S., 2011. Engineering cyber infrastructure for U-Pb geochronology: Tripoli and U-Pb_Redux. Geochemistry, Geophysics, Geosystems 12, http://dx.doi.org/10.1029/2010GC003479.

Broderick, C., Wotzlaw, J., Frick, D., Gerdes, A., Ulianov, A., Günther, D., Schaltegger, U., 2015. Linking the thermal evolution and emplacement history of an upper-crustal pluton to its lower-crustal roots using zircon geochronology and geochemistry (southern Adamello batholith, N. Italy). Contributions to Mineralogy and Petrology 170, 1-17.

Burnham, A.D., Berry, A.J., 2012. An experimental study of trace element partitioning between zircon and melt as a function of oxygen fugacity. Geochimica et Cosmochimica Acta 95, 196-212.

Burnham, C.W., Ohmoto, H., 1980. Late-stage processes of felsic magmatism. Soc. Mining Geol. Jpn. 8, 1-11.

Candela, P., 1989. Magmatic ore-forming fluids: thermodynamic and mass transfer calculations of metal concentrations. Reviews in Economic Geology 4, 203-221.

Cathles, L., 1977. An analysis of the cooling of intrusives by ground-water convection which includes boiling. Economic Geology 72, 804-826.

Cathles, L., Shannon, R., 2007. How potassium silicate alteration suggests the formation of porphyry ore deposits begins with the nearly explosive but barren expulsion of large volumes of magmatic water. Earth and Planetary Science Letters 262, 92-108.

Charlier, B., Bachmann, O., Davidson, J., Dungan, M., Morgan, D., 2007. The upper crustal evolution of a large silicic magma body: evidence from crystal-scale Rb–Sr isotopic heterogeneities in the Fish Canyon magmatic system, Colorado. Journal of Petrology 48, 1875-1894.

Chelle-Michou, C., Chiaradia, M., Ovtcharova, M., Ulianov, A., Wotzlaw, J.-F., 2014. Zircon petrochronology reveals the temporal link between porphyry systems and the magmatic evolution of their hidden plutonic roots (the Eocene Coroccohuayco deposit, Peru). Lithos 198, 129-140.

Cherniak, D., Hanchar, J., Watson, E., 1997a. Diffusion of tetravalent cations in zircon. Contributions to Mineralogy and Petrology 127, 383-390.

Cherniak, D., Hanchar, J., Watson, E., 1997b. Rare-earth diffusion in zircon. Chemical Geology 134, 289-301.

Chiaradia, M., Schaltegger, U., Spikings, R., Wotzlaw, J.-F., Ovtcharova, M., 2013. How accurately can we date the duration of magmatic-hydrothermal events in porphyry systems?—an invited paper. Economic Geology 108, 565-584.

Claiborne, L.L., Miller, C.F., Flanagan, D.M., Clynne, M.A., Wooden, J.L., 2010. Zircon reveals protracted magma storage and recycling beneath Mount St. Helens. Geology 38, 1011-1014.

Coleman, D.S., Gray, W., Glazner, A.F., 2004. Rethinking the emplacement and evolution of zoned plutons: Geochronologic evidence for incremental assembly of the Tuolumne Intrusive Suite, California. Geology 32, 433-436.

Condon, D., Schoene, B., McLean, N., Bowring, S., Parrish, R., 2015. Metrology and traceability of U-Pb isotope dilution geochronology (EARTHTIME Tracer Calibration Part I). Geochimica et Cosmochimica Acta 164, 464-480.

Deering, C., Bachmann, O., 2010. Trace element indicators of crystal accumulation in silicic igneous rocks. Earth and Planetary Science Letters 297, 324-331.

Dilles, J.H., 1987. Petrology of the Yerington Batholith, Nevada; evidence for evolution of porphyry copper ore fluids. Economic Geology 82, 1750-1789.

Dilles, J.H., Kent, A.J., Wooden, J.L., Tosdal, R.M., Koleszar, A., Lee, R.G., Farmer, L.P., 2015. Zircon compositional evidence for sulfur-degassing from ore-forming arc magmas. Economic Geology 110, 241-251.

Ferry, J., Watson, E., 2007. New thermodynamic models and revised calibrations for the Ti-in-zircon and Zr-in-rutile thermometers. Contributions to Mineralogy and Petrology 154, 429-437.

Glazner, A.F., Bartley, J.M., Coleman, D.S., Gray, W., Taylor, R.Z., 2004. Are plutons assembled over millions of years by amalgamation from small magma chambers? GSA today 14, 4-12.

560 Halter, W.E., Bain, N., Becker, K., Heinrich, C.A., Landtwing, M., Von Quadt, A., Clark, A.H., Sasso, A.M.,
561 Bissig, T., Tosdal, R.M., 2004a. From andesitic volcanism to the formation of a porphyry Cu-Au
562 mineralizing magma chamber: the Farallón Negro Volcanic Complex, northwestern Argentina. Journal of
563 Volcanology and Geothermal Research 136, 1-30.
564 Halter, W.E., Heinrich, C.A., Pettke, T., 2004b. Laser-ablation ICP-MS analysis of silicate and sulfide melt
565 inclusions in an andesitic complex II: evidence for magma mixing and magma chamber evolution.
566 Contributions to Mineralogy and Petrology 147, 397-412.
567 Halter, W.E., Heinrich, C.A., Pettke, T., 2005. Magma evolution and the formation of porphyry Cu–Au ore
568 fluids: evidence from silicate and sulfide melt inclusions. Mineralium Deposita 39, 845-863.
569 Harris, A.C., Allen, C.M., Bryan, S.E., Campbell, I.H., Holcombe, R.J., Palin, J.M., 2004a. ELA-ICP-MS U–
570 Pb zircon geochronology of regional volcanism hosting the Bajo de la Alumbrera Cu–Au deposit:
571 implications for porphyry-related mineralization. Mineralium Deposita 39, 46-67.
572 Harris, A.C., Kamenetsky, V.S., White, N.C., Steele, D.A., 2004b. Volatile phase separation in silicic
573 magmas at Bajo de la Alumbrera porphyry Cu-Au deposit, NW Argentina. Resource Geology 54, 341-356.
574 Hattori, K., 1993. High-sulfur magma, a product of fluid discharge from underlying mafic magma: evidence
575 from Mount Pinatubo, Philippines. Geology 21, 1083-1086.
576 Hattori, K.H., Keith, J.D., 2001. Contribution of mafic melt to porphyry copper mineralization: evidence
577 from Mount Pinatubo, Philippines, and Bingham Canyon, Utah, USA. Mineralium Deposita 36, 799-806.
578 Hofmann, A.E., Valley, J.W., Watson, E.B., Cavosie, A.J., Eiler, J.M., 2009. Sub-micron scale distributions
579 of trace elements in zircon. Contributions to Mineralogy and Petrology 158, 317-335.
580 Huber, C., Bachmann, O., Vigneresse, J.L., Dufek, J., Parmigiani, A., 2012. A physical model for metal
581 extraction and transport in shallow magmatic systems. Geochemistry, Geophysics, Geosystems 13.
582 Llambías, E., 1972. Estructura del grupo volcanico Farallon Negro, Catamarca, Republica Argentina. Revista
583 de la Asociacion Geologica Argentina 27, 161-169.
584 Mattinson, J.M., 2005. Zircon U–Pb chemical abrasion ("CA-TIMS") method: combined annealing and
585 multi-step partial dissolution analysis for improved precision and accuracy of zircon ages. Chemical Geology
586 220, 47-66.

587 Mattinson, J.M., 2011. Extending the Krogh legacy: development of the CA-TIMS method for zircon U-Pb
588 geochronology This article is one of a series of papers published in this Special Issue on the theme of
589 Geochronology in honour of Tom Krogh. Canadian Journal of Earth Sciences 48, 95-105.
590 Matzel, J.E., Bowring, S.A., Miller, R.B., 2006. Time scales of pluton construction at differing crustal levels:
591 Examples from the Mount Stuart and Tenpeak intrusions, North Cascades, Washington. Geological Society
592 of America Bulletin 118, 1412-1430.
593 McLean, N., Bowring, J., Bowring, S., 2011. An algorithm for U-Pb isotope dilution data reduction and
594 uncertainty propagation. Geochemistry, Geophysics, Geosystems 12,
595 http://dx.doi.org/10.1029/2010GC003478.
596 McLean, N.M., Condon, D.J., Schoene, B., Bowring, S.A., 2015. Evaluating uncertainties in the calibration
597 of isotopic reference materials and multi-element isotopic tracers (EARTHTIME Tracer Calibration Part II).
598 Geochimica et Cosmochimica Acta 164, 481-501.
599 Memeti, V., Paterson, S., Matzel, J., Mundil, R., Okaya, D., 2010. Magmatic lobes as "snapshots" of magma
600 chamber growth and evolution in large, composite batholiths: An example from the Tuolumne intrusion,
601 Sierra Nevada, California. Geological Society of America Bulletin 122, 1912-1931.
602 Mercer, C.N., Reed, M.H., Mercer, C.M., 2015. Time scales of porphyry Cu deposit formation: insights from
603 titanium diffusion in quartz. Economic Geology 110, 587-602.
604 Miller, J.S., Matzel, J.E., Miller, C.F., Burgess, S.D., Miller, R.B., 2007. Zircon growth and recycling during
605 the assembly of large, composite arc plutons. Journal of Volcanology and Geothermal Research 167, 282-
606 299.
607 Miller, C.F., Furbish, D.J., Walker, B.A., Claiborne, L.L., Koteas, G.C., Bleick, H.A., Miller, J.S., 2011.
608 Growth of plutons by incremental emplacement of sheets in crystal-rich host: evidence from Miocene
609 intrusions of the Colorado River region, Nevada, USA. Tectonophysics 500, 65-77.
610 Nadeau, O., Stix, J., Williams-Jones, A.E., 2013. The behavior of Cu, Zn and Pb during magmatic-
611 hydrothermal activity at Merapi volcano, Indonesia. Chemical Geology 342, 167-179.
612 Ohnenstetter, D., Cesbron, F., Remond, G., Caruba, R., Claude, J.-M., 1991. Émissions de
613 cathodoluminescence de deux populations de zircons naturels: tentative d'interprétation. Comptes rendus de
614 l'Académie des sciences. Série 2, Mécanique, Physique, Chimie, Sciences de l'univers, Sciences de la Terre
615 313, 641-647.

Proffett, J.M., 2003. Geology of the Bajo de la Alumbrera porphyry copper-gold deposit, Argentina. Economic Geology 98, 1535-1574.

Reid, M.R., Vazquez, J.A., Schmitt, A.K., 2011. Zircon-scale insights into the history of a Supervolcano, Bishop Tuff, Long Valley, California, with implications for the Ti-in-zircon geothermometer. Contributions to Mineralogy and Petrology 161, 293-311.

Rivera, T.A., Schmitz, M.D., Crowley, J.L., Storey, M., 2014. Rapid magma evolution constrained by zircon petrochronology and $^{40}Ar/^{39}Ar$ sanidine ages for the Huckleberry Ridge Tuff, Yellowstone, USA. Geology 42, 643-646.

Rubatto, D., Hermann, J., 2007. Experimental zircon/melt and zircon/garnet trace element partitioning and implications for the geochronology of crustal rocks. Chemical Geology 241, 38-61.

Samperton, K.M., Schoene, B., Cottle, J.M., Keller, C.B., Crowley, J.L., Schmitz, M.D., 2015. Magma emplacement, differentiation and cooling in the middle crust: Integrated zircon geochronological–geochemical constraints from the Bergell Intrusion, Central Alps. Chemical Geology 417, 322-340.

Sasso, A., Clark, A., 1998. The Farallón Negro Group, northwest Argentina: magmatic, hydrothermal and tectonic evolution and implications for Cu-Au metallogeny in the Andean back-arc. Society of Economic Geologists Newsletter 34, 8-18.

Schaltegger, U., Brack, P., Ovtcharova, M., Peytcheva, I., Schoene, B., Stracke, A., Marocchi, M., Bargossi, G.M., 2009. Zircon and titanite recording 1.5 million years of magma accretion, crystallization and initial cooling in a composite pluton (southern Adamello batholith, northern Italy). Earth and Planetary Science Letters 286, 208-218.

Schmitz, M.D., Bowring, S.A., 2001. U-Pb zircon and titanite systematics of the Fish Canyon Tuff: an assessment of high-precision U-Pb geochronology and its application to young volcanic rocks. Geochimica et Cosmochimica Acta 65, 2571-2587.

Schmitz, M.D., Schoene, B., 2007. Derivation of isotope ratios, errors, and error correlations for U‐Pb geochronology using 205Pb‐235U‐(233U)‐spiked isotope dilution thermal ionization mass spectrometric data. Geochemistry, Geophysics, Geosystems 8, http://dx.doi.org/10.1029/2006GC001492.

Schoene, B., Guex, J., Bartolini, A., Schaltegger, U., Blackburn, T.J., 2010a. Correlating the end-Triassic mass extinction and flood basalt volcanism at the 100 ka level. Geology 38, 387-390.

644 Schoene, B., Latkoczy, C., Schaltegger, U., Günther, D., 2010b. A new method integrating high-precision
645 U–Pb geochronology with zircon trace element analysis (U–Pb TIMS-TEA). Geochimica et Cosmochimica
646 Acta 74, 7144-7159.
647 Schoene, B., Schaltegger, U., Brack, P., Latkoczy, C., Stracke, A., Günther, D., 2012. Rates of magma
648 differentiation and emplacement in a ballooning pluton recorded by U-Pb TIMS-TEA, Adamello batholith,
649 Italy. Earth and Planetary Science Letters 355, 162-173.
650 Sillitoe, R.H., 2010. Porphyry copper systems. Economic Geology 105, 3-41.
651 Smoliar, M.I., Walker, R.J., Morgan, J.W., 1996. Re-Os ages of group IIA, IIIA, IVA, and IVB iron
652 meteorites. Science 271, 1099.
653 Steinberger, I., Hinks, D., Driesner, T., Heinrich, C.A., 2013. Source plutons driving porphyry copper ore
654 formation: combining geomagnetic data, thermal constraints, and chemical mass balance to quantify the
655 magma chamber beneath the Bingham Canyon deposit. Economic Geology 108, 605-624.
656 Tapster, S., Condon, D., Naden, J., Noble, S., Petterson, M., Roberts, N., Saunders, A., Smith, D., 2016.
657 Rapid thermal rejuvenation of high-crystallinity magma linked to porphyry copper deposit formation;
658 evidence from the Koloula Porphyry Prospect, Solomon Islands. Earth and Planetary Science Letters 442,
659 206-217.
660 Trail, D., Tailby, N.D., Lanzirotti, A., Newville, M., Thomas, J.B., Watson, E.B., 2015. Redox evolution of
661 silicic magmas: Insights from XANES measurements of Ce valence in Bishop Tuff zircons. Chemical
662 Geology 402, 77-88.
663 Trail, D., Watson, E.B., Tailby, N.D., 2012. Ce and Eu anomalies in zircon as proxies for the oxidation state
664 of magmas. Geochimica et Cosmochimica Acta 97, 70-87.
665 Ulrich, T., Heinrich, C.A., 2002. Geology and alteration geochemistry of the porphyry Cu-Au deposit at Bajo
666 de la Alumbrera, Argentina. Economic Geology 97, 1865-1888.
667 Von Quadt, A., Erni, M., Martinek, K., Moll, M., Peytcheva, I., Heinrich, C.A., 2011. Zircon crystallization
668 and the lifetimes of ore-forming magmatic-hydrothermal systems. Geology 39, 731-734.
669 von Quadt, A., Wotzlaw, J.-F., Buret, Y., Large, S.J., Peytcheva, I., Trinquier, A., 2016. High-precision
670 zircon U/Pb geochronology by ID-TIMS using new 10^{13} ohm resistors. Journal of Analytical Atomic
671 Spectrometry 31, 545-822.

672 Wallace, P.J., 2005. Volatiles in subduction zone magmas: concentrations and fluxes based on melt inclusion
673 and volcanic gas data. Journal of Volcanology and Geothermal Research 140, 217-240.
674 Wark, D., Hildreth, W., Spear, F., Cherniak, D., Watson, E., 2007. Pre-eruption recharge of the Bishop
675 magma system. Geology 35, 235-238.
676 Watson, E., Harrison, T., 2005. Zircon thermometer reveals minimum melting conditions on earliest Earth.
677 Science 308, 841-844.
678 Watson, E., Wark, D., Thomas, J., 2006. Crystallization thermometers for zircon and rutile. Contributions to
679 Mineralogy and Petrology 151, 413-433.
680 Weis, P., Driesner, T., Heinrich, C., 2012. Porphyry-copper ore shells form at stable pressure-temperature
681 fronts within dynamic fluid plumes. Science 338, 1613-1616.
682 Wendt, I., Carl, C., 1991. The statistical distribution of the mean squared weighted deviation. Chemical
683 Geology: Isotope Geoscience Section 86, 275-285.
684 Wotzlaw, J.-F., Schaltegger, U., Frick, D.A., Dungan, M.A., Gerdes, A., Günther, D., 2013. Tracking the
685 evolution of large-volume silicic magma reservoirs from assembly to supereruption. Geology 41, 867-870.
686 Zajacz, Z., Halter, W., 2009. Copper transport by high temperature, sulfur-rich magmatic vapor: Evidence
687 from silicate melt and vapor inclusions in a basaltic andesite from the Villarrica volcano (Chile). Earth and
688 Planetary Science Letters 282, 115-121.

689 # Figure Captions

690 Figure 1: Cross section 49N of the Bajo de la Alumbrera showing the mine surface in 2008. All rocks above
691 this level have been mined. Pre-mineralisation porphyries (Los Amarillos porphyry; LAP) and volcanics
692 (undifferentiated andesites) are shown in white. Copper grades are shown in colours, while dated porphyry
693 intrusions are differentiated by patterns. The location of the Farallón Negro volcanic complex (FNVC) is
694 shown in the map of Argentina.
695
696 Figure 2: Rock slab from Bajo de la Alumbrera showing early P2 porphyry that solidified before becoming
697 veined and altered (pervasive quartz – magnetite) before the precipitation of 4 cm quartz-chalcopyrite vein,
698 which was then cross-cut by the unmineralised LP3 porphyry. Abbreviations: cp = chalcopyrite; qz = quartz.
699

Figure 3: Age ranked plot showing all concordant $^{206}Pb/^{238}U$ dates for individual zircons and Re-Os molybdenite dates. Weighted mean age is given based on the youngest statistically equivalent populations for each sample. Expanded uncertainties on the weighted mean ages (e.g. ± x/y) include tracer and decay constant uncertainties for direct comparison between the Re-Os and U-Pb dates.

Figure 4: (a-c) Variations of trace element concentrations and ratios of zircon through time of whole grains analysed by CA-ID-TIMS; d) Zircon Hf-isotopic compositions through time.

Figure 5: Cathodoluminescence images of zircon showing locations of trace element analysis spots and corresponding trace element data. (a) P4 type 1 zircon; (b) P4 type 2 zircon; (c) LP3 type 1 zircon; (d) LP3 type 2 zircon; (e) EP3 type 1 zircon); (f) EP3 type 2 zircon; (g) P2 type 1 zircon; (h) P2 type 2 zircon. Scale bars = 50 μm.

Figure 6: LA-ICP-MS trace element data for cores, rims and "dark-zones" of zircon grains from the pre-mineralisation P2 and post-mineralisation LP3 porphyries. Fields of bulk-grain TIMS-TEA results are indicated by black dashed lines. Ti-in-zircon temperatures are calculated using $a_{TiO2} = 0.7$ and $a_{SiO2} = 1$ (Ferry and Watson, 2007). For plots of EP3 and P4 see Supplementary Materials Figure 1.

Figure 7: Uranium concentrations for zircon cores and rims (by LA-ICP-MS) and for whole zircons grains that were dated by CA-IDTIMS are low and constant, whereas black zones are variably high in U, as well as in other trace elements shown in Figure 8.

Figure 8: LA-ICP-MS trace element data for zircons from the post-mineralisation LP3 CL images from a LP3 zircon (insets a) shows the locations of the trace element analysis spots and corresponding trace element data; (b) Core-rim tie-lines (arrows) point towards fractional crystallisation; (c) Core-"dark-zone" tie-lines (green arrows) and "dark-zone"-rim tie-lines (red arrows) show that the "dark-zones" do not follow fractional crystallisation trends. Light grey fields show the location of all the data shown in (a), whereas dark grey fields show the location of the majority of the data shown in (a). (See Fig. 6 for legend).

729 Figure 9: Conceptual model for zircon crystallisation for the Bajo de la Alumbrera deposit (not to scale); (a)
730 Initial composite magma chamber (indicated by different colours) at 7.35 Ma crystallised zircon at ~ 750 °C
731 displaying simple growth zoning. This magma chamber quickly reached an immobile state (indicated by +
732 symbols); (b) Following a mafic recharge event into the base of the magma chamber an exsolved CO_2-rich
733 vapour was released into the immobile felsic crystal mush. Zircons which crystallised from melt modified by
734 the CO_2-rich vapour phase underwent rapid crystallisation recorded as "dark-zones". Zircons which grew
735 from melt that was not modified by the CO_2 rich vapour continued to crystallise in equilibrium with the melt.
736 As a result of increased crystallinities, the vapour phase formed fast migration pathways to the apical parts of
737 the magma chamber; (c) Pressure build-up at the top of the magma body resulted in the sudden pulses of
738 magma and fluid release in quick succession. Zircons were "tapped" from different parts of the magma
739 chamber, and rims with fine growth zoning overgrew both zircon types prior to the cooling of the porphyries.
740 Focussed fluid release led to the formation of the ore-shell (striped area). See section 5.4 for discussion.

Figure

Click here to download Figure: Figure_1.pdf

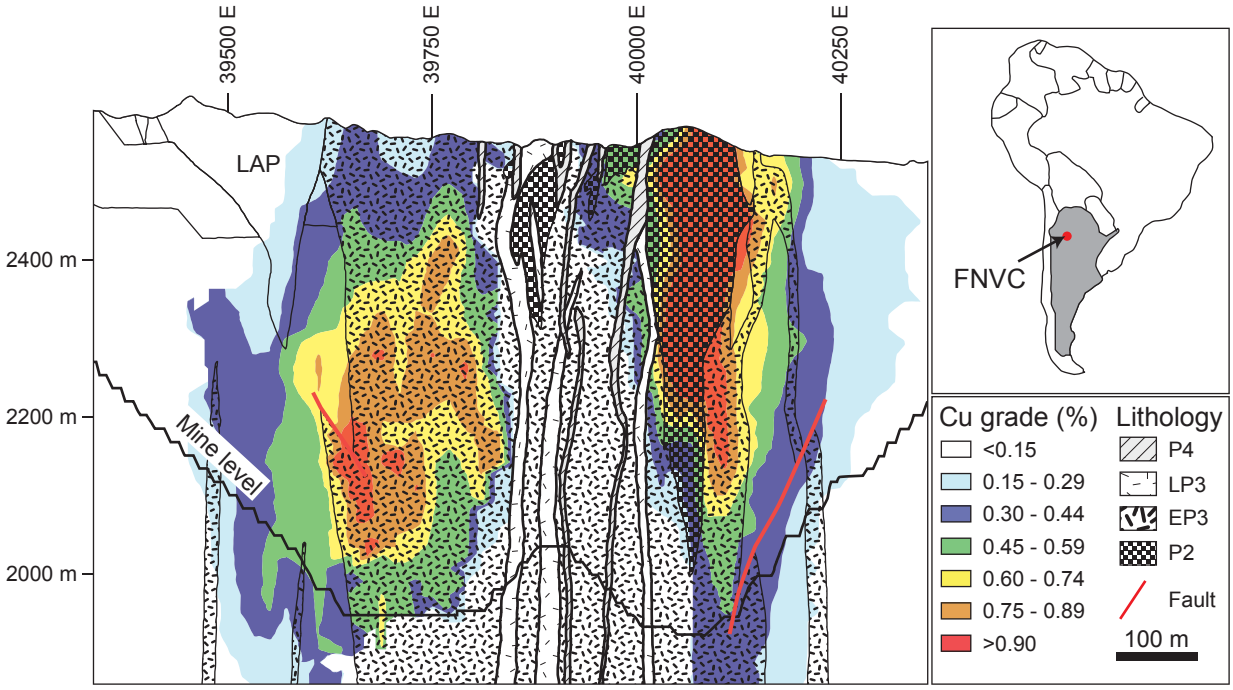

Figure

Click here to download Figure: Figure_2.pdf

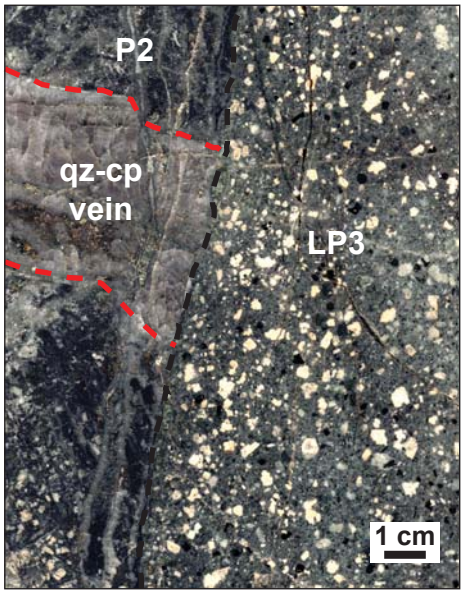

Figure

Click here to download Figure: Figure_3.pdf

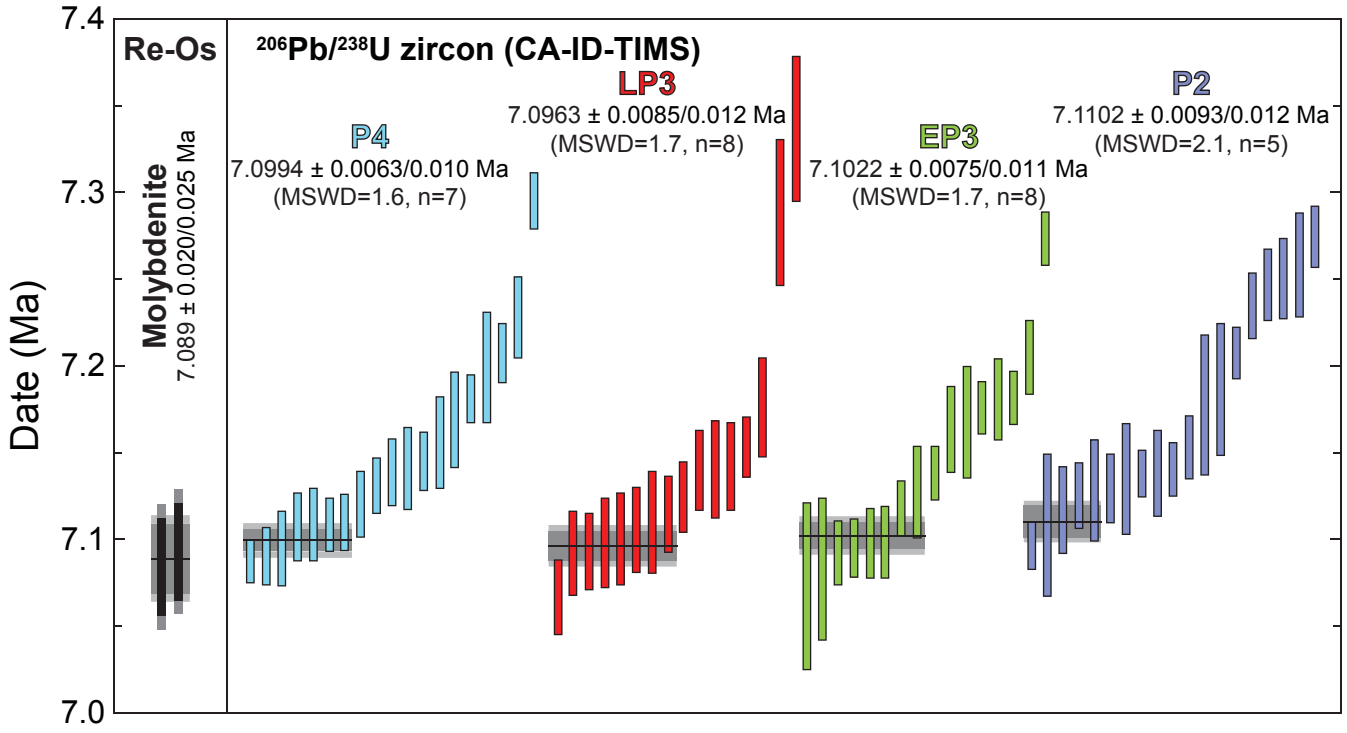

Figure

Click here to download Figure: Figure_4.pdf

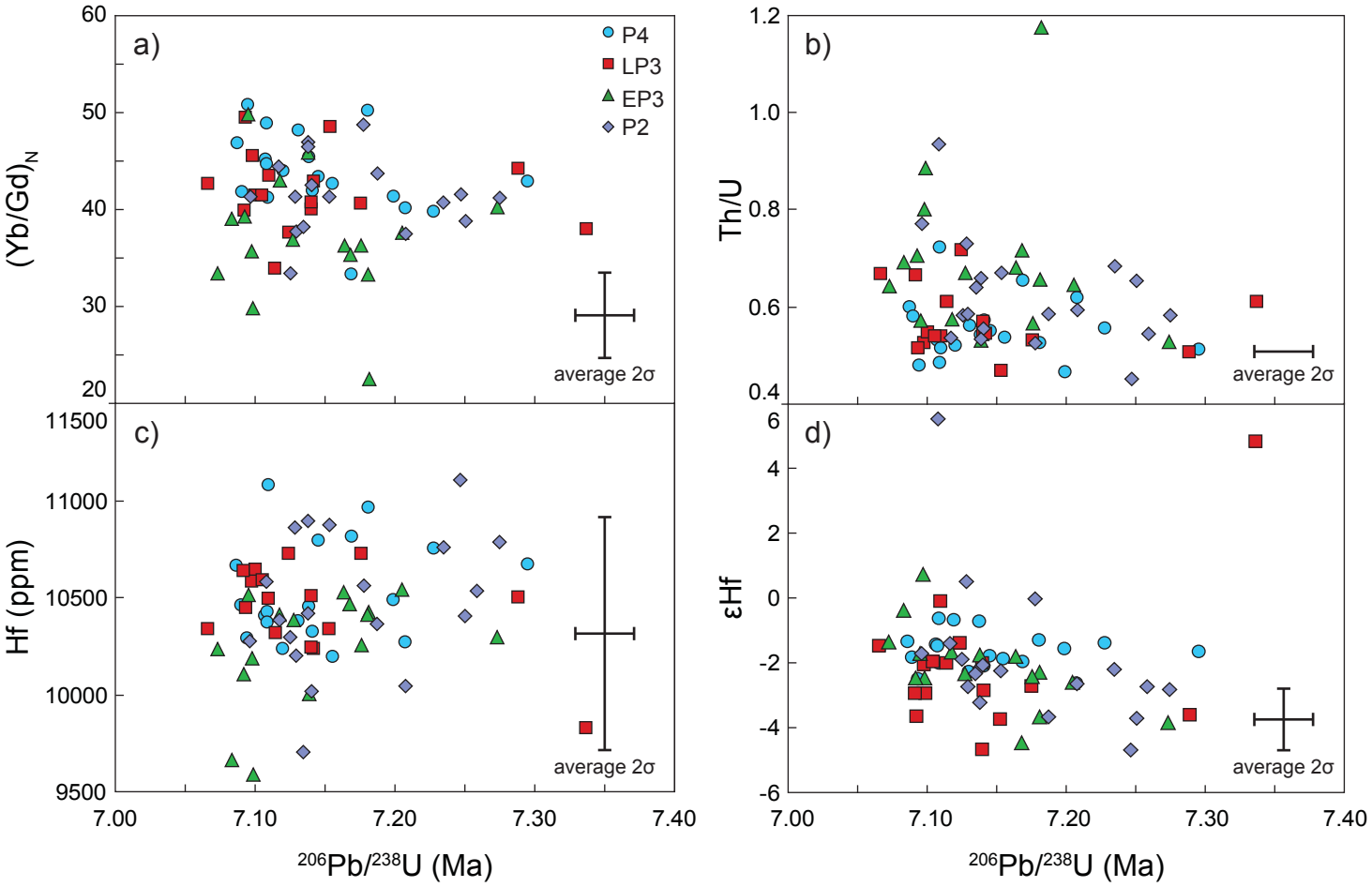

Figure

Click here to download Figure: Figure_5.pdf

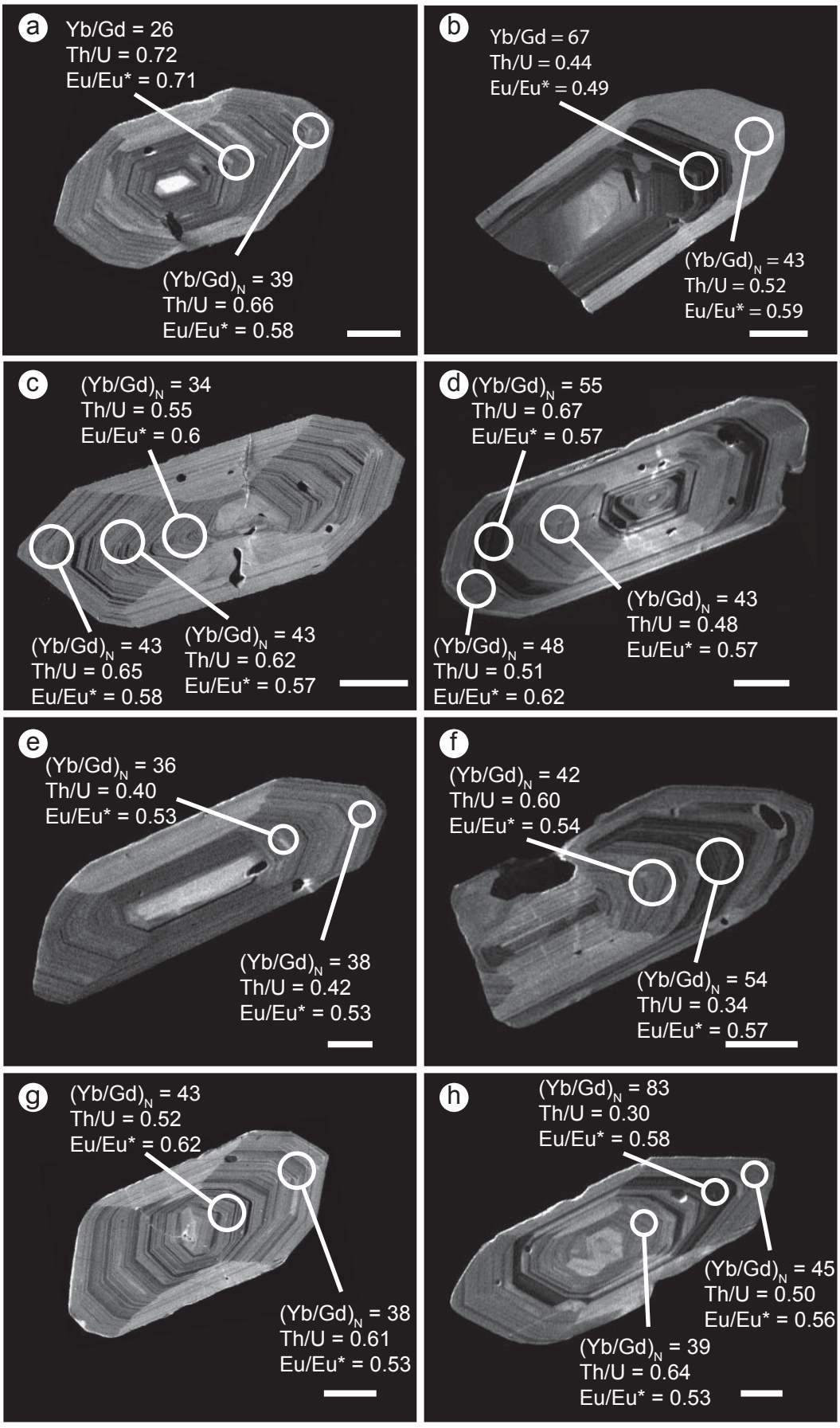

Figure

Click here to download Figure: Figure_6.pdf

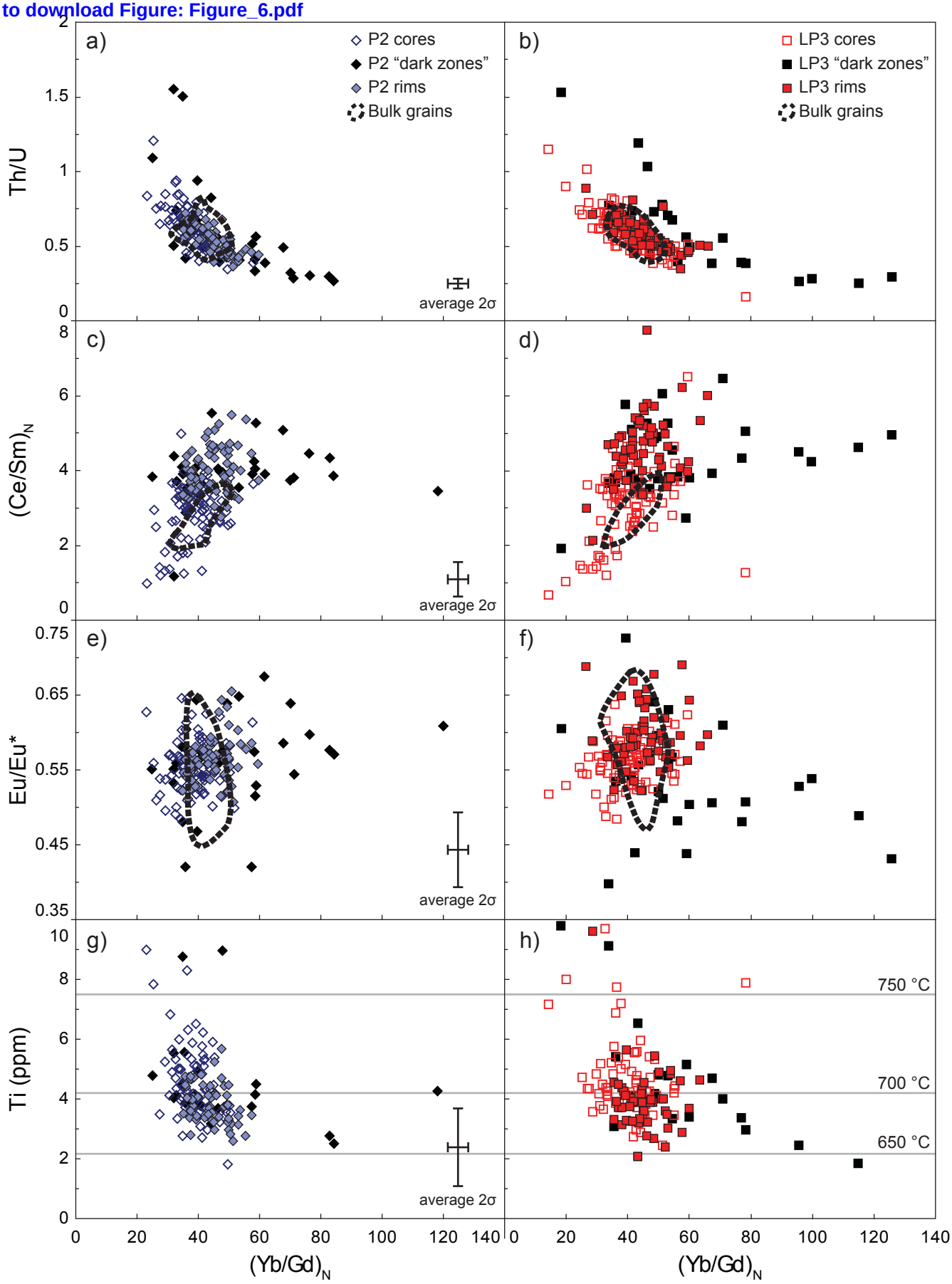

Figure

Click here to download Figure: Figure_7.pdf

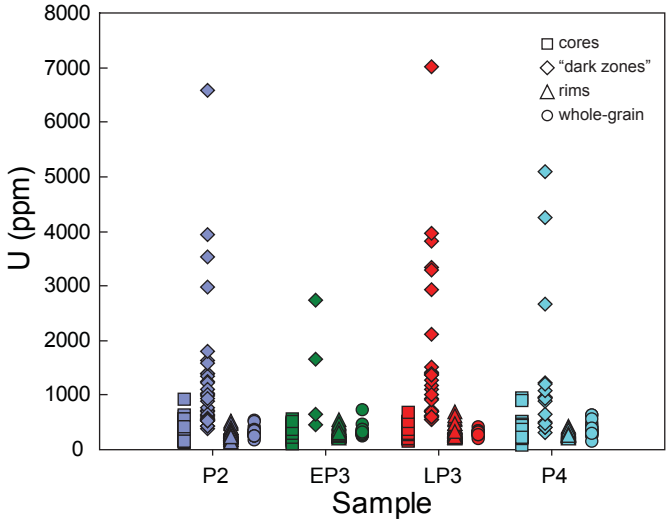

Figure

Click here to download Figure: Figure_8.pdf

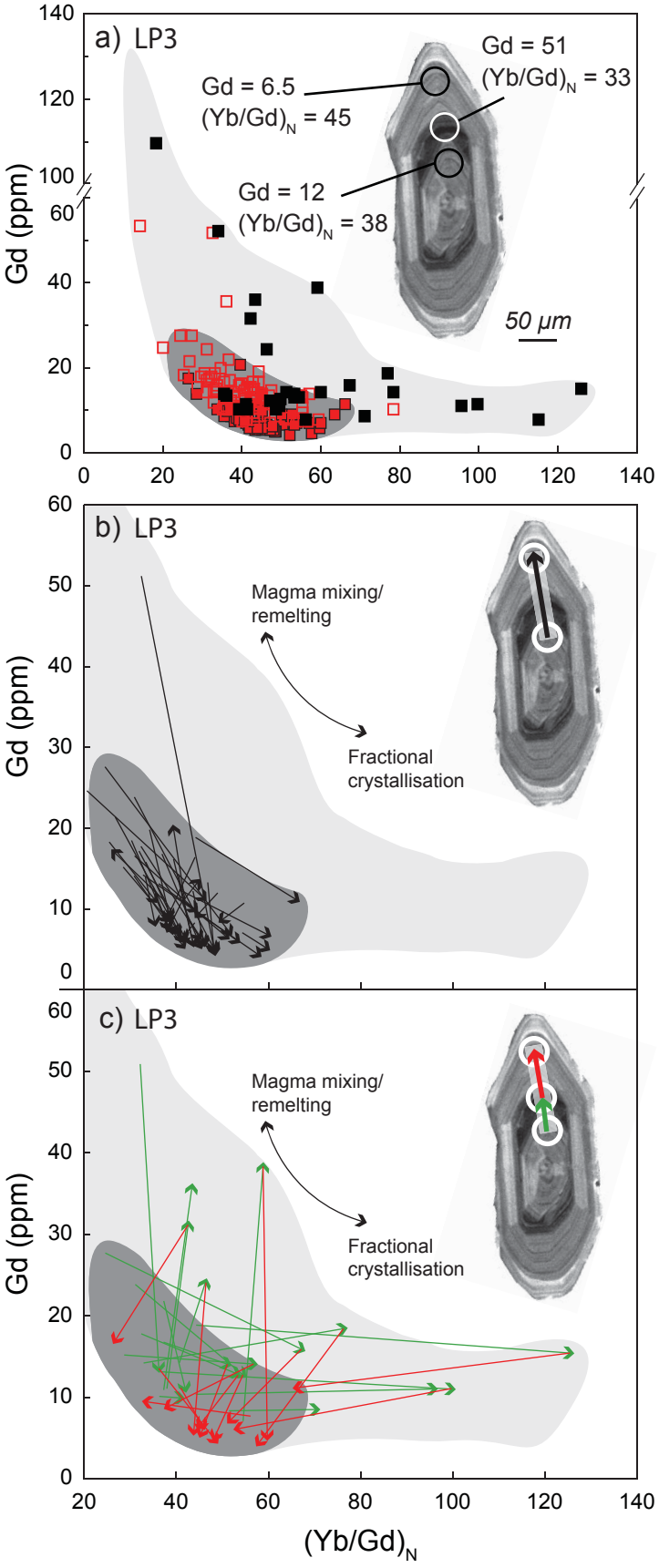

Figure

Click here to download Figure: Figure_9.pdf

a) ~7.35 Ma: Zircon saturation @ 750 °C within a composite upper-crustal magma chamber

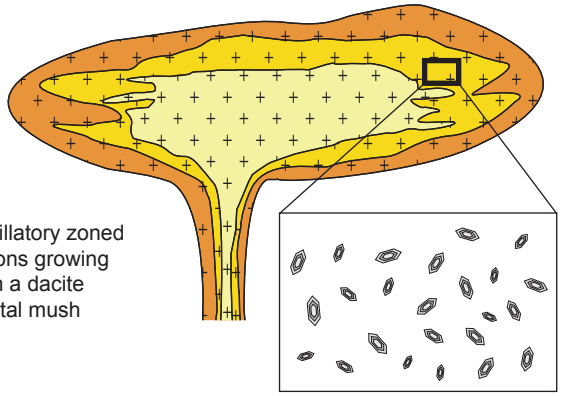

Oscillatory zoned zircons growing from a dacite crystal mush

b) Injected andesitic magma releases vapour phase which forms channels and rises to the apex of the magma chamber

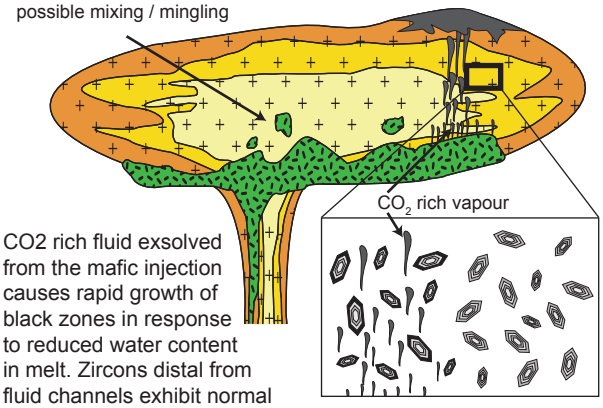

CO2 rich fluid exsolved from the mafic injection causes rapid growth of black zones in response to reduced water content in melt. Zircons distal from fluid channels exhibit normal growth zoning

c) ~7.1 Ma: Fluid overpressure results in the rapid formation of the porphyry copper deposit within a few 10,000 years or less

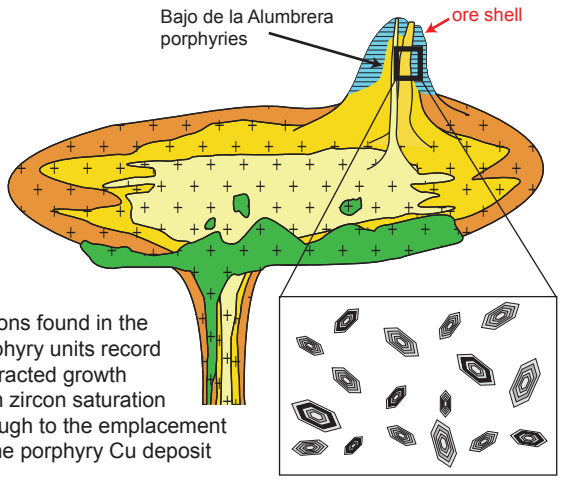

Zircons found in the porphyry units record protracted growth from zircon saturation through to the emplacement of the porphyry Cu deposit